2020 IEEE/RSJ International Conference on Intelligent Robots and Systems (IROS)
October 25-29, 2020, Las Vegas, NV, USA (Virtual)

Subsurface Sampling Robot for Time-limited Asteroid Exploration

Hiroki Kato, Yasutaka Satou, Kent Yoshikawa, Masatsugu Otsuki, Hirotaka Sawada,
Takeshi Kuratomi and Nana Hidaka

Abstract— **This paper presents a novel approach to sampling subsurface asteroidal regolith under severe time constraints. Sampling operations that must be completed within a few hours require techniques that can manage subsurface obstructions that may be encountered. The large uncertainties due to our lack of knowledge of regolith properties also make sampling difficult. To aid in managing these challenges, machine learning-based detection methods using tactile feedback can detect the presence of rocks deeper than the length of the probe, ensuring reliable sampling in unobstructed areas. In addition, given the variability of soil hardness and the short time available, a corer shooting mechanism has been developed that uses a special shape-memory alloy to collect regolith in about a minute. Experiments on subsurface obstacle detection and shooting-corer ejection tests were conducted to demonstrate the functionality of this approach.**

I. INTRODUCTION

Sample return missions from an asteroid are subject to severe time limitations. Martian Moons eXploration (MMX) is JAXA's next sample return mission being developed, and will make a landing on Phobos in order to conduct detailed scientific observation [1]. The sampling robot will collect regolith from the surface layer to a depth of more than two centimeters, and the entire sampling procedure must be finished within 2.5 hours.

Returning a scientifically valuable subsurface regolith poses technical challenges, such as the rigid time limit and considerable lack of knowledge about regolith terramecanical properties and embedded subsurface obstructions. Under such circumstances, a sampling mechanism must be designed in concert with a proper mission operation sequence. Particularly when regolith samples are taken from below the surface, determining the presence of subsurface rocks that cannot be detected from camera imagery is critical.

This paper presents a new time-limited method of subsurface sampling for asteroid exploration using a combination of tactile subsurface inspection using machine learning and a coring shooting mechanism. Before coring, a tactile subsurface inspection is conducted using a thin rod to detect underground rocks by predicting the distance between the tip of the rod and the existing rock. Based on the transfer of force inside the layers of regolith, rock under the ground produces a boundary effect, which is too complex to model or identify significant parameters. Although the terramechanical parameters are too uncertain, making it too difficult to model, the resultant force influenced by the boundary effect of rocks can be learned. The support vector machine (SVM) operates by measuring the force of pushing a short, thin rod a few centimeters in diameter into the regolith. To perform subsurface sampling, a corer shooting mechanism uses a single crystal shape memory alloy (SCSMAs) as an actuator. The corer can acquire subsurface regolith with a quick, single ejection within a minute. The sampling robot will be able to use the corer shooting mechanism to probe at rock-free locations with the ability to inspect subsurface rock, thereby ensuring the collection of samples of regolith.

The rest of this paper is organized as follows: Section II describes related works, including the prospective mission requirements. Section III explains the proposed subsurface sampling method, including the tactile subsurface inspection that is described in Section IV. The corer shooting mechanism is covered in Section V. Section VI evaluates the performance of the proposed method, and Section VII presents the conclusions of this paper.

II. RELATED WORKS

A. Small-body sampling

The asteroid sample return mission is subject to strict time limitations for sampling operation so as to ensure the survival of the spacecraft return module. Such previous sample return missions, including JAXA's Hayabusa mission [2], and its successor mission Hayabusa 2 [3], adapted a touch-and-go approach. Sampling was done within a few seconds after the flexible sampler mechanism touched the asteroid surface to trigger a projectile launched at the surface regolith and producing impact emissions. Similarly, NASA's OSIRIS-REx mission will collect samples by injecting nitrogen gas into surface regolith during a touch-and-go operation [4].

Although there are only a few flight-proven cases of small-body sampling, prospective candidates for the sampling mechanism include a drill [5][6], that with percussion [7], a projectile [2][3], a pneumatic system [4][8], and a corer [9][10][11].

B. Terrain inspection

If there is a rock in the regolith, the sampling mechanism will bounce back and fail to obtain a sample, but a robot with the ability to inspect subsurface rock, could shoot the coring mechanism at rock-free locations. Another reason to use terrain inspection during wheeled rover exploration: sandy, soft regolith increases the risk of getting stuck [12]. In addition, In addition, a legged robot stepping on subsurface

H. Kato[1], Y. Satou[2], K. Yoshikawa[2], M. Otsuki[2], and H. Sawada[2] are with Japan Aerospace Exploration Agency (JAXA). T. Kuratomi[3] and N. Hidaka[3] are with WEL Research Co., Ltd. [1] 2-1-1 Sengen, Tsukuba, Ibaraki, JAPAN 305-8505 / [2] 3-1-1 Yoshinodai, Sagamihara, Kanagawa, JAPAN 252-5210 / [3] 212-11 Aoyagi, Ichihara, Chiba 299-0102, and kato.hiroki@jaxa.jp

rock would significantly change the control profile and could topple, thereby damaging itself [13]-[18].

There is literature on the inspection of planetary terrain surface regolith. Terramechanics is studied to establish the traction control of a planetary rover, with sinkage and shear being modeled and characterized [19] [20] [21]. The same applies to a legged robot [22]. However, it is very difficult to estimate terramechanical parameters for regolith, and subsurface rock detection has yet to be achieved.

Given the difficulty posed by the modeling, machine learning could be a reasonable approach to terrain classification. An attempt was made to apply this method to planetary rover applications that use sensor data, such as vibration data and visual information for learning [23] [24]. Reference [13] attempted to classify underground rock but failed because they could not discriminate between soil with and without rock, as well as rock with and without soil.

Thus far, the classification of subsurface rock has yet to be achieved. Moreover, general field robotics applications investigate terrain classification with various learning methods, including the use of a neural network and a support vector machine [14]-[18]. However, they only support classification by surface materials (e.g., carpet, building floor, dirt, sand). For the sake of safety, Kolvenbach et al. suggest that a legged robot use its limbs to inspect the terrain before taking a suspicious step [13]. This naturally includes subsurface inspection. In subsurface sampling, a short, thin rod with as little mass as possible but with a force sensor is pushed into ground to probe for the presence of rocks before penetration.

C. Requirements for subsurface sampling

MMX, planned to launch in the year of 2024, will make a landing on Phobos in order to make detailed scientific observations [1]. Although the proposed method is applicable to other subsurface sampling missions, a prospective mission requirement from the Martian moon sampling robot can be examined.

The MMX mission will need to acquire samples of at least 10 grams of regolith at a time. In addition, the sampling robot shall collect regolith from at least two centimeters below the surface. Moreover, the sampling robot shall collect regolith in 2.5 hours because the spacecraft is not prepared for overnight operation. As other procedures must be carried out, such as settling the landed spacecraft and checking the communication link, sampling actions shall be completed in a minute or less. The regolith could be compacted, and the samples taken where they are not obstructed by subsurface rock. After all, the sampling operation must be done in an unknown environment at the landing site.

III. Proposed Subsurface Sampling Method

Given the requirements presented in Subsection II-C, this section first describes sampling method selection, and then proposes the sampling method.

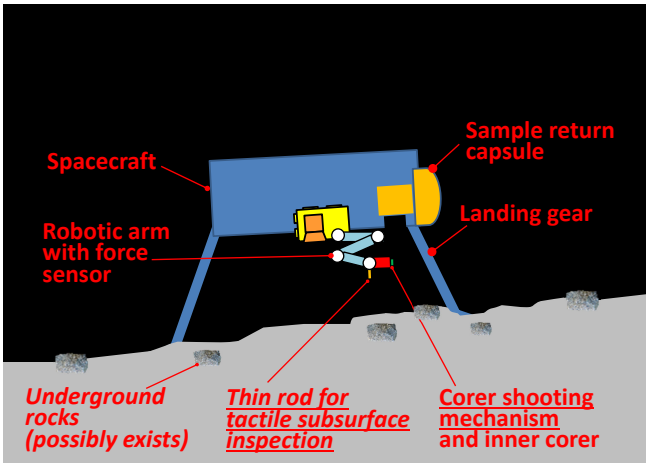

Fig. 1. Subsurface sampling robot hardware

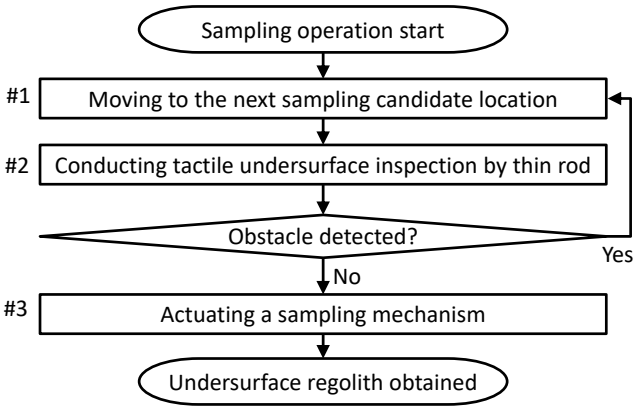

Fig. 2. The mission sequence of subsurface inspection

A. Sampling method selection

Subsection II-A describes the sampling methods, and these options are carefully compared because the sampling mechanism selection and its detailed design depend on the these requirements.

If the sample mass is more than ten grams, projectile-based sampling (limited to several grams) cannot be used. Also, drilling and percussion are eliminated as sampling mechanism candidates because both require much more than a minute to do. In addition, the requirement of collecting regolith from a depth of at least two centimeters eliminates the pneumatic option.

A coring mechanism can obtain a sample even when the regolith of the landing site is compacted, so a corer shooting mechanism meets all the requirements. Note that preserving the order of regolith layers is not requirement, as it will be shaken and destroyed during the Earth reentry phase of the mission

B. Sampling approach using tactile subsurface inspection and shooting coring mechanism

Figure 1 depicts the robot hardware for asteroid subsurface sampling. The sampling robot is equipped with a robotic arm that can move to desired sampling locations. The robotic arm has an end effector with a coring mechanism. The robotic arm collects regolith from the ground by ejecting the

collector then transfers the sample to the return capsule. The regolith is encapsulated by the shooting coring mechanism installed on the end effector. For subsurface inspection, a force sensor and thin rod a few centimeters in diameter are installed on the base of the end effector.

Figure 2 shows the sampling sequence for tactile subsurface inspection. Initially, the robotic arm moves the coring mechanism to the first or next sampling location (step #1 in Fig. 2) by the robotic arm. Next, the thin rod penetrates the ground for tactile subsurface inspection (step #2 in Fig. 2). If there is any large rock in the ground within the injection distance, the coring mechanism will bounce off and not obtain regolith. To avoid this, the robot pushes a thin rod with into the ground to investigate whether there are any subsurface rocks before injection as described in Section IV. Note that the reaction force due to pushing ground by the robotic arm shall be small enough not to push the spacecraft up from the surface. If an underground obstacle is detected within the range of corer penetration, the tip of the robotic arm is moved to the next location. If no underground obstacle is detected, the inner corer is shot at that location (step #3 in Fig. 2). Thus, a sufficient amount of subsurface regolith can be obtained there due to the absence of obstacles.

IV. Tactile Subsurface Inspection

Following the prospective scenario of tactile subsurface inspection as described in the previous section, this section depicts the associated methodology using a thin rod on the end effector of the robot arm, the boundary effect, the dataset collection, feature selection, and classification method.

A. Rod-regolith interaction and boundary effect phenomena

Understanding the physics of tactile subsurface inspection by using a thin rod entails two parts: (1) interaction between a thin rod and regolith, and (2) interactions of the thin rod, regolith, and a boundary.

First, the interaction between a thin rod and regolith is described. A thin rod is pushed into regolith quasi-statically and penetrates its subsurface. For a thin rod with a flat tip, frictional force operates between the end of the thin rod and the regolith, and the regolith cannot freely deform horizontally. The regolith just below acts as a wedge-shaped rigid body attached to the bottom of the thin rod [25]. which is how the thin rod can push deeply through the regolith. Verified from this phenomenon, the ultimate bearing capacity applied to the wedge-shaped rigid body (q)—the maximum pressure that can be supported without failure—is modeled by Terzaghi's bearing capacity equation [25]:

$$q = 1.3 * cN_c + \gamma_2 D_f N_q + 0.3 * \gamma_1 B N_\gamma, \qquad (1)$$

where c is cohesion (N/m^2), D_f is the pushed distance from the surface (m), B is the base width of the thin rod (m), N_c, N_q and N_γ are bearing capacity factors, unitless terramechanical parameters depending on the regolith's internal friction angle, and γ_1 and γ_2 are appropriate unit weight of regolith (N/m^3). This equation clearly shows that the force reacting to the bottom of the thin rod is linearly

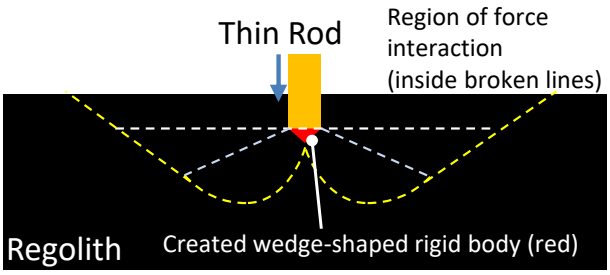

Fig. 3. Rod-regolith interaction sketch from simplified Terzaghi's model

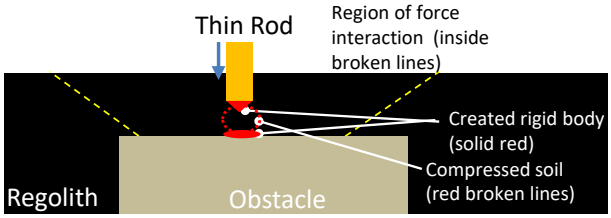

Fig. 4. Simplified sketch of boundary effect

proportional to the distance pushed in from the surface, D_f. Note that the second and third terms depend on the mass of the regolith, so it has less effect in microgravity, and the force due to the rod-regolith interaction becomes dominant. Although we do not describe this phenomenon in further detail, Terzaghi's model shows the pushed force interacting over a wide area as shown in Fig. 3. A wedge-shaped rigid body attached to the bottom of the thin rod (the red area in the figure) is created due to the friction between the surface of the bottom of the thin rod and the regolith and to compression of the regolith. The wedge-shaped body presses the regolith of the area between the gray and yellow lines causing radial shear flow. This regolith pushes the regolith outside the area between while and yellow lines above the gray line. In summary, the regolith inside the yellow line is affected by the inserted thin rod.

Finally, the boundary effect (i.e., interactions of thin rod, regolith, and a boundary) is described. When inserted, the thin rod compresses the bottom regolith into a hard wedge shape and pushes the surrounding material, but if there is a boundary object such as a rock or the bottom of the container, the nearby regolith that cannot escape is firmly compacted as seen in Fig. 4. It is beyond our scope to model the boundary effect though, given such interacting forces, magnitude of reaction force depends on depth as well as the distance between the tip of the thin rod and the existing obstacle, which will become the learning parameter of our machine-learning approach.

B. Machine learning

The physics from the previous subsection can describe the reaction force in the rod's direction of extension depends on the depth of the thin rod as well as the distance to the obstacle. It contains sufficient information to detect the presence of rocks. Such data can be collected by using a force sensor on the base of the thin rod's end effector. For simplicity, the thin rod is cylindrical with a flat base, and

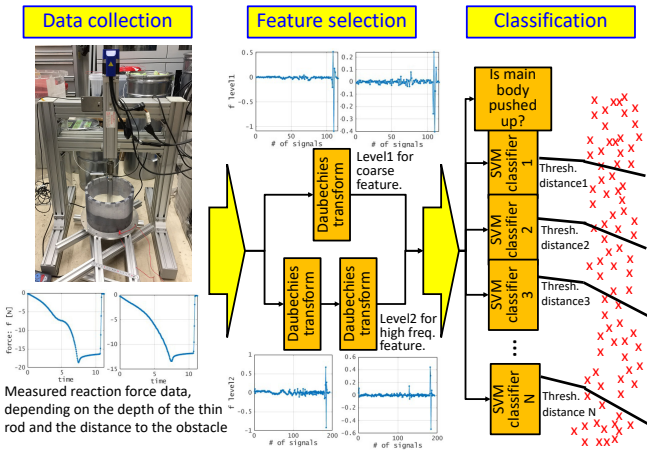

Fig. 5. Machine learning overview for tactile subsurface inspection

is slowly pushed into the ground regolith. Fig. 5 shows a machine learning procedure consisting of feature selection and classification, as described in the rest of this subsection.

(1) Feature selection

As the applied motor torque is controllable, the measurements of force and its rate of change can be used as key features for classification. The Daubechies transform (Daub4) [26], a discrete wavelet transform (DWT), is applied to enhance signal interpretation. The Daubechies transform is well known for containing both time domain information and frequency domain information in a minimum data size. For a slowly applied force, the Daub4 level-1 signals are intended for representing coarse information, using both the approximation coefficient and detail (fluctuation) coefficient of the Daubechies transform with a relatively low sampling frequency. For the Daub4 level-2 signals, only detail coefficients with a slightly higher sampling frequency are used to observe the frequency domain. In fact, the Daub4 level-3 signals contain little information and thus are not used.

(2) Classification

The features generated in the previous subsection are fed to a classifier. Here, a support vector machine (SVM) is used because of its relatively low computation cost for prediction, which is important to spacecraft applications. The SVM can distinguish only between two classes. As the features depend on the distance from the boundary, it is possible to identify features as either ”close” or ”far,” depending on the threshold distance. By applying the SVM classification with different threshold distances, the distance to the boundary from the tip of the thin rod is predicted, although this incurs an additional computation cost.

V. *Corer shooting mechanism design*

A simplistic corer mechanism is widely proposed for planetary sampling purposes. Our corer shooting mechanism (Fig. 6) generates a large ejection energy for the smallest possible volume. Its shooting actuator is made of TiNi™ SC-SMA Components, a special shape memory alloy by Ensign-Bickford Aerospace and Defence [27]. When it transforms by heat, the rate of instantaneous volume change is nine

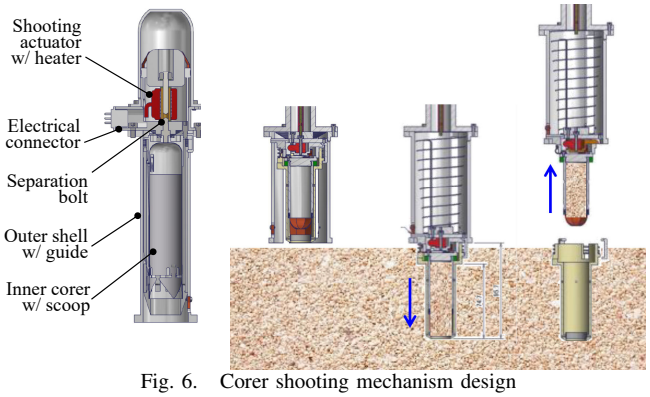

Fig. 6. Corer shooting mechanism design

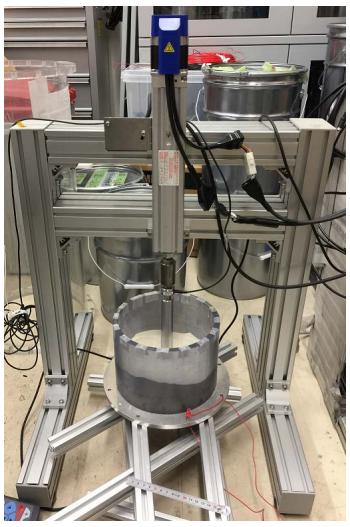

Fig. 7. The experiment setup - a probing system testbed

percent, yielding an extremely large ejection energy capable of breaking a separation bolt and shooting out the inner corer with an attached scoop. It takes less than a minute for the shooting operation, satisfying the mission requirement. The ejection energy of the corer mechanism is set for the prospective regolith with the most compact case. Depending on the hardness of the regolith and the presence of obstacles, the tip of the inner corer can reach deeper than required, while simultaneously collecting regolith.

VI. Experimental Results

The first subsection shows the evaluation of inspecting for subsurface obstacles, then the corer shooting mechanism's ability to collect subsurface samples in an obstacle-free location is evaluated.

A. *Evaluation of tactile subsurface inspection*

The sampling robot shall inspect subsurface rock to shoot the corer shooting mechanism. Fig. 7 shows the probing system testbed used in the experiment. A precision linear actuator by Keyence with a maximum stroke distance of 100 millimeters is placed on a relatively heavy outer frame. A 500N-strain gauge (LUR-A-500N) by Kyowa is installed on the base of the linear actuator connected with the outer frame. A thin aluminum rod is placed on the tip of the

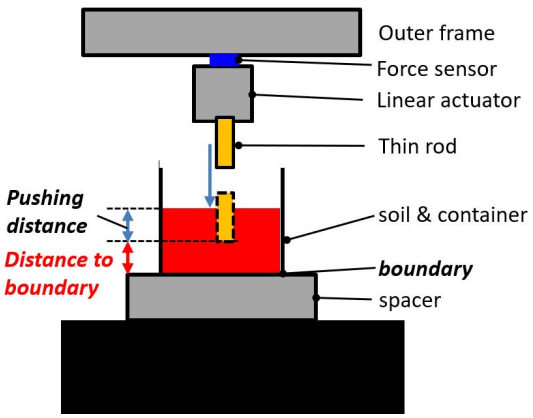

Fig. 8. The boundary height and regolith surface configuration

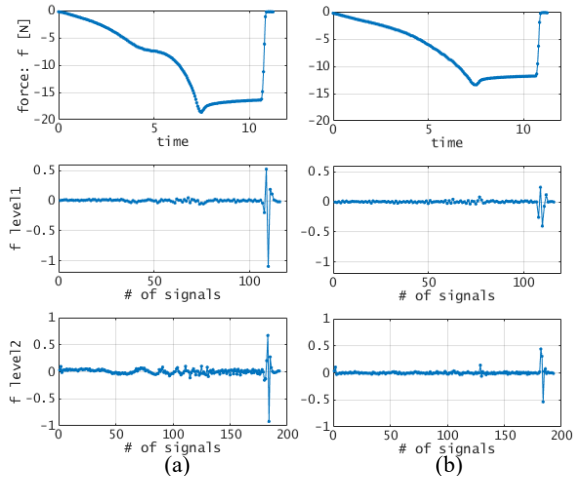

Fig. 9. The Daubechies transformed force signal, comparison of with and without boundary effect

linear actuator to apply force to the regolith. The thin rod is 20 mm in diameter. A regolith container is placed so that the thin rod pushes into the center of the surface. Spacer blocks are placed under the regolith container to control the height of the boundary (i.e., the aluminum base of the regolith container). For dataset collection, Fig. 8 shows the configuration of the boundary height and regolith surface.

(1) Comparison of with and without boundary effect

Figure 9 compares the signals with (Fig. 9 (a)) and without (Fig. 9 (b)) the base of the boundary effect. In the trial, a force was slowly applied to the regolith until the tip of the rod is 40 millimeters into the regolith. It remains there for three seconds, and then is slowly extracted. For (a), the flat boundary is placed 54 mm from the surface (which is 14 millimeters deeper than the tip of the inserted rod). For (b), the flat boundary is 100 mm from the surface. In (a), it is clearly shown that measured force increases drastically as the tip of the thin rod approaches the boundary, which is also observed by the Daubechies-transformed signals. Moreover, the Daubechies-transformed level-2 signal in (a) shows more change than the one in (b). The sampling frequencies in the figure are 20 Hz for level 1 and 67 Hz for level 2; this may depend on the speed of the thin rod penetration.

Note that the rate of measured force in (a) and (b) increases as the tip of the rod penetrates deeper. In (b), although the rate would not change in terms of depth in Terzaghi's model, the rate of measured force, in fact, differs slightly in each trial without the boundary. The regolith is mixed and leveled gently and evenly before each trial, as the regolith is assumed to be compact of loose. It is too difficult to reproduce the case. In (a), the further acceleration of measured force is observed, and more drastic change in both in the level1 and level2 signals are appeared.

(2) Tactile subsurface object detection

For each trial, the height of the spacers and the stroke distance of the linear actuator are adjusted to achieve the desired distance to the boundary. Also, the amount of regolith inside the container is adjusted for each trial so that the pushing distance (height) inside the regolith is between 30 and 41 millimeters. In addition, the regolith is mixed and leveled gently and evenly before each trial.

It is important to note that we did not collect data with a distance to the boundary shorter than 12 mm for machine learning purposes. This is because with a shorter distance to the boundary, the reaction force becomes so high that the outer frame is pushed up. This may also occur in the Martian Moons exploration mission, where Phobos is 0.0005G. This situation would be easily detected by the spacecraft's onboard IMU when underground rocks have been detected. Thus, this case is omitted for detection by machine learning.

Fig. 10 shows typical force sensor data profiles from the experiment. The linear actuator moves at 5 millimeters per second. Once the tip of the thin rod reaches the desired position, it stops for three seconds. Then it withdraws at 5 millimeters per second. Eventually, the measured force drops back to zero newtons, and the tip of the thin rod is extracted from the regolith. When the tip of the thin rod reaches the desired position, the force reaches the lowest peak. Based on the force signal reading, we search for its local minima. Letting the time at the local minima t_p, force sensor data between $t_p - 5.0$ seconds and $t_p + 3.8$ seconds are extracted for further processing, as described in the subsection on feature selection (from *"original f"* to *"extracted f"* in Fig. 10). Consequently, the number of features for the descriptor is 333 (91 for level-1 approximation coefficient, 91 for level-1 detailed coefficient, and 151 for level-2 detailed coefficient).

Table I summarizes the experiment cases. Each case has a different threshold. The learning classes (" close" or " far") are labeled according to the comparison of the distance to the boundary and the threshold distance. In each case, cross validation with a randomly chosen test size of 0.20 is conducted five times to examine accuracy. After all, sci-kit learn [28] is used to implement SVM.

Table II lists the classification confusion matrices for each case. The results show that the closer the threshold value, the higher the accuracy. When the threshold is smaller than 18 millimeters (Cases 1 - 3), it has 100% accuracy. This result is intuitively true because, according to the boundary

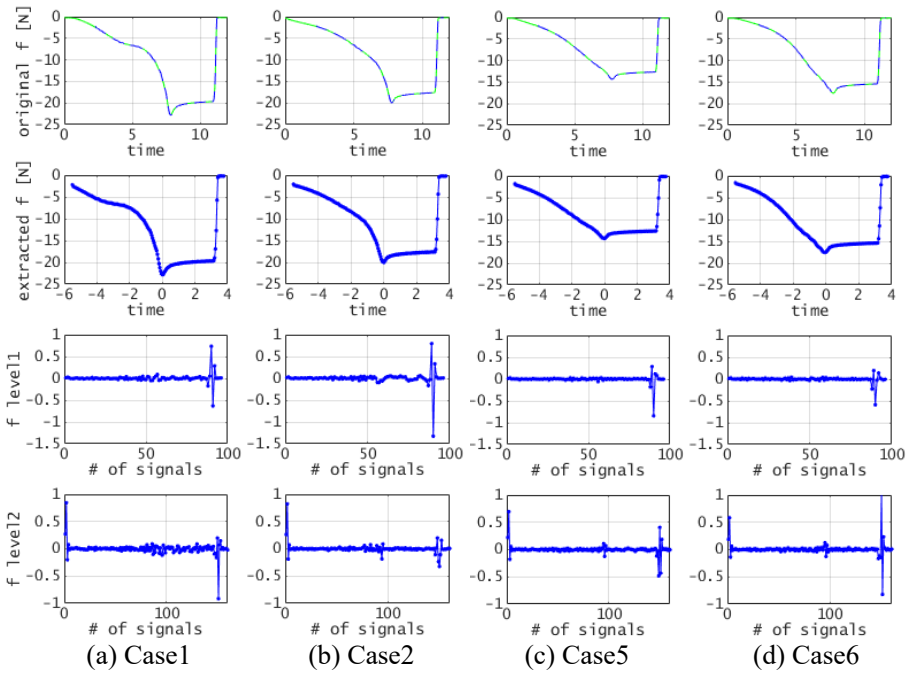

Fig. 10. Typical force sensor data profile from the experiment

TABLE I

SUMMARY OF THE EXPERIMENT CASES

Dist. to boundary (mm)	# of trials	Case 1	Case 2	Case 3	Case 4	Case 5	Case 6
12	23	close	close	close	close	close	close
14	24	far	close	close	close	close	close
16	9	far	far	close	close	close	close
18	10	far	far	far	close	close	close
20	10	far	far	far	far	close	close
22	14	far	far	far	far	far	close
24	15	far	far	far	far	far	far
Threshold (mm)		14	16	18	20	22	24

effect physics, a higher reaction force is applied to the near boundary. It is also reasonable that the boundary effect is lost when the boundary is far enough away (Cases 5 and 6), which can be observed in (c) and (d) of Fig. 10. Thus, classification results in lower accuracy at a high threshold distance to the boundary. In addition, the accuracy becomes worse in between those cases (Case 4). To summarize the experimental results, at most the case of 18 millimeters of the boundary effect is predicted successfully, and the accuracy gets worse for higher distance to the boundary.

B. Evaluation of corer shooting mechanism

The purpose of the experiment in this subsection is to show the corer shooting mechanism propels the ejected inner corer to penetrate the regolith while quantitatively controlling individual differences of the mechanism.

Figure 11 shows the experiment setup. The corer-shooting mechanism is placed to the relatively heavy outer frame.

TABLE II

SUMMARY OF THE EXPERIMENT RESULT

Case	Thresh. (mm)	actual ↓	predicted close	predicted far	accuracy %
1	14	close	29	0	100
		far	0	76	
2	16	close	47	0	100
		far	0	58	
3	18	close	55	0	100
		far	0	50	
4	20	close	68	2	97.1
		far	1	34	
5	22	close	70	6	90.5
		far	4	25	
6	24	close	83	5	88.6
		far	7	10	

TABLE III

THE RESULT FOR CORER SHOOTING MECHANISM EVALUATION

Trial #	1	2	3	4	5
Generated velocity [m/sec]	4.9	4.9	5.2	5.2	4.1
Kinetic energy [J]	2.2	2.2	2.5	2.5	1.5
Penetration depth [mm]	95&	73	39	95&	95&

& The inner corer is penetrated completely.

Applying heat to the actuator heater, the inner corer with its mass of 184 grams is shot. The corer shooting mechanism is eventually mounted on the tip of a highly stiff robotic arm. The reaction force will be generated during the shooting of the inner corer, and it may be transmitted to the spacecraft, causing the spacecraft to turn over. Although the magnitude

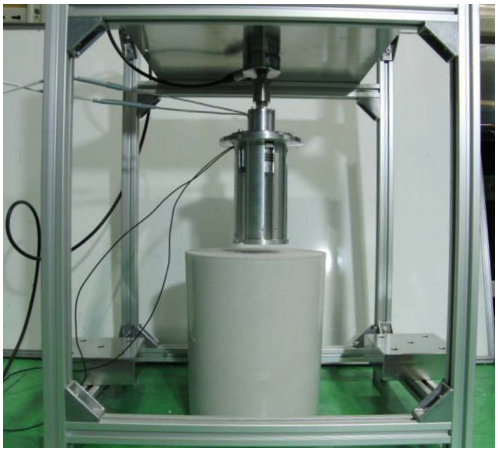

Fig. 11. The experiment setup for corer shooting mechanism evaluation

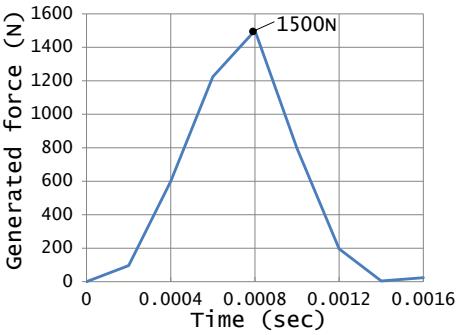

Fig. 12. The transient response of generated force by the corer shooting mechanism (from Trial #1)

of the transferred reaction force depends on the design of the robotic arm, it is critical to measure the generated force. A 2000N-strain gage (LUR-A-SA1) by Kyowa is installed on the base of the corer shooting mechanism connected with the outer frame. The force measuring system has a sampling rate of 5kHz. The inner corer accelerates instantaneously while the SCSMA stretches a few millimeters, yielding the initially generated velocity. By measuring the transient response of generated force, the initially generated velocity of the ejected inner corer is calculated. It enables quantitatively controlling individual differences of the corer shooting mechanism by kinetic energy. The tip of the corer is placed to about ten millimeters apart from the surface of the regolith. When they are further apart, the ejected inner corer does not penetrate the ground straight under the influence of the Earth's gravity and air. The inner corer is shot into a bucket filled with sand of sufficient depth. The sand depth of the reached inner corer tip is measured. Note also that silica sand with a particle size of about 50-100 micrometers (similar to the predicted particle size distribution on Phobos) is used for the entire experiment.

Figure 12 shows a typical transient response of generated force by the corer shooting mechanism. The generated force is measured for less than 1.4 milliseconds with its peak of 1500 Newton. Since the peak force would depend on mechanical stiffness of the strain gauge mount, the ability of ejection should be evaluated either impulse (0.88 Newton-second in this trial) or kinetic energy (2.2 joules). In addition, it takes between twenty and forty seconds for heating up the shape memory alloy to trigger shooting under the ambient room temperature. The result also meets the system requirement to actuate for sampling within a minute.

Table III shows the overall result from the experiment. The kinetic energy between 1.5 and 2.5 joules is generated by the corer shooting mechanism, and penetration depth of more than two centimeters is achieved in all trials. Trial #5 has least kinetic energy among the trials, but the inner corer is completely penetrated. Also, Trial #3 has least penetration depth, but the kinetic energy of the trial is larger than in the other trials. In Trial #3, the hardness of the sand was found to be harder around the surface, although it is only a qualitative observation. Given the sufficient kinetic energy provided by the corer-shooting mechanism, the penetration depth is estimated to significantly depend on the hardness of the surface. Although the sand bucket was leveled as evenly as possible, it is still difficult to control the bulk density of the sand as [13] mentions.

VII. Conclusion

This work proposed a subsurface sampling method for Phobos under severe time constraints and our lack of knowledge of the surface and subsurface regolith conditions using a combination of the SVM-based tactile subsurface inspection and the SCSMA-based corer shooting mechanism. First, with the corer shooting mechanism, prospective sampling sequence for the asteroid exploration mission is presented, where existence of subsurface obstacles is inspected with an equipped thin rod, and they are avoided by the equipped robotic arm. The reaction force profile under the regolith surface is introduced using rod-regolith interaction and boundary effect physics, including Terzaghi's model, although these complex terramechanical parameters need not be identified. The transient profile of the reaction force depends on depth as well as the distance between the tip of the thin rod and the existing obstacle, which can be used for machine learning approach. As training data of the SVM approach, the measurement of force and its rate of change are collected, and the Daubechies transform is applied to extract features from the signal. The experimental results show that at most the 18-millimeter case of the boundary effect is predicted successfully, and that the accuracy gets worse for greater distances to the boundary. Then the corer-shooting mechanism with an actuator that can acquire subsurface regolith with a quick, single ejection, is designed. Al-though it depends on the initial surrounding temperature, it is likely to shoot within a minute. For subsurface coring experiment, a kinetic energy between 1.5 and 2.5 joules is generated by the designed corer-shooting mechanism, and penetration depth of more than two centimeters was achieved in all trials.

For future work, it is necessary to cope with the uncertainties of planetary exploration. Although regolith parameters, such as particle size and bulk density, are used for the experiment in our work, the actual parameters will not

be unveiled except at the target planet. It is necessary to establish a methodology to create controlled bulk density and a related parametric study should be conducted for both the subsurface coring mechanism and tactile subsurface inspection. Also, the effect of the boundary shape must be considered, as the shape of rocks can affect the consolidation of regoliths at their boundaries. Moreover, effects of microgravity must be studied. Drop-tower testing could be done to actuate the corer mechanism with the correlated kinetic energy, but it may be difficult to repeat hundreds of times for parametric study and to obtain data for machine learning. To overcome the situation, a dynamic simulation model of regolith and our devices must be developed. The dynamic simulation should enable the investigation of different ground conditions, including the regolith's bulk density and local inclination of the ground surface.

REFERENCES

[1] Y. Kawakatsu, et. al., "Mission Design of Martian Moons eXploration (MMX)." Proceedings of International Astronautical Congress (IAC), Washington D. C., U.S.A., 2019.

[2] H. Yano, et. al., "Touchdown of the Hayabusa Spacecraft at the Muses Sea on Itokawa." Science, vol. 312, pp. 1350-1353, 2006.

[3] H. Sawada, et. al., "Hayabusa2 Sampler: Collection of Asteroidal Surface Material." Space Science Reviews, vol. 208, no.1-4, pp. 81-106, 2017.

[4] D.S. Lauretta, et. al., "OSIRIS-REx: sample return from Asteroid (101955) Bennu." Space Science Reviews, col. 212, pp. 925-984, 2017.

[5] Y. Bar-Cohen, and K. Zacny, "Drilling in Extreme Environments: Penetration and Sampling on Earth and other Planets." Wiley-VCH, Weinheim, 2009.

[6] W. Watanabe, et. al., "A Mole-type Drilling Robot for Lunar Subsurface Exploration." Proceedings of International Symposium on Artificial Intelligence and Robotics and Automation in Space, Nara, Japan, AS-7, 2003.

[7] R. C. Anderson, et. al., "Collecting Samples in Gale Crater, Mars; an Overview of the Mars Science Laboratory Sample Acquisition, Sample Processing and Handling System." Space Science Reviews, vol. 170, pp. 57-75, 2012.

[8] K. Zacny, et. al. "Pneumatic Sampler (P-Sampler) for the Martian Moons eXploration (MMX) Mission." Proceedings of IEEE Aerospace Conference, Big Sky, MT, 2020. (To be appeared.)

[9] S.W. Squyres, et. al., "The Athena Mars rover science payload." Lunar Planetary Science, Vol. 29, pp.1101–1102. 1998.

[10] Y. Bar-Cohen, et. al., "Ultrasonic/sonic driller/corer (USDC) as a sampler for planetary exploration," Proceedings of IEEE Aerospace Conference, Big Sky, MT, pp. 263-271, 2001.

[11] D. Agnolon, "Study overview of the near earth asteroid sample return." European Space Agency SCI-PA/2007/004/PA, 2007.

[12] G. Webster and V. McGregor, Nasa's mars rover has uncertain future as sixth anniversary nears, December 2009. https://mars.nasa.gov/mer/newsroom/pressreleases/20091231a.html (Accessed Sept. 5th, 2019)

[13] H. Kolvenbach, et. al. "Haptic Inspection of Planetary Soils with Legged Robots." in Proceedings of IEEE International Conference on Robotics and Automation (ICRA), Montreal, pp. 1626-1632, 2019.

[14] K. Walas, "Terrain classification and negotiation with a walking robot," Journal of Intelligent and Robotic Systems, vol. 78, no. 3, pp. 401-423, 2015.

[15] J. Mrva and J. Faigl, "Feature extraction for terrain classification with crawling robots," Information Technologies - Applications and Theory (ITAT), vol. 1422, pp. 179-185, 2015.

[16] M. Hoffmann, et. al.,"The effect of motor action and different sensory modalities on terrain classification in a quadruped robot running with multiple gaits," Robotics and Autonomous Systems, vol. 62, no. 12, pp. 1790 -1798, 2014.

[17] K. Walas, "Tactile sensing for ground classification," Journal of Automation, Mobile Robotics and Intelligent Systems, vol. 7, pp. 18, 2013.

[18] P. Kozlowski, K. Walas, "Deep Neural Networks for Terrain Recognition Task," Baltic URSI Symposium (URSI), 2018.

[19] J. Wong and A. Reece, "Prediction of rigid wheel performance based on the analysis of soil-wheel stresses part i. performance of driven rigid wheels," Journal of Terramechanics, vol. 4, no. 1, pp. 81 98, 1967.

[20] M. Sutoh, et. al., "Traveling and abrasion characteristics of wheels for lunar exploration rover in vacuum," Journal of Terramechanics, vol. 68, no. 12, pp. 37-49, 2016.

[21] C. Cunningham, I. Nesnas, and W. Whittaker, "Improving slip prediction on mars using thermal inertia measurements, Robotics Science and Systems" (RSS), 2017.

[22] L. Ding, et al., "Foot-terrain interaction mechanics for legged robots: Modeling and experimental validation," The International Journal of Robotics Research, vol. 32, no. 13, pp. 15851606, 2013.

[23] C. Brooks and K. Iagnemma, "Vibration-based terrain classification for planetary exploration rovers," IEEE Transactions on Robotics, vol. 21, no. 6, pp. 11851191, 2005.

[24] I. Halatci, C. A. Brooks, and K. Iagnemma, "Terrain classification and classifier fusion for planetary exploration rovers," IEEE Aerospace Conference, pp. 111, 2007.

[25] K. Terzaghi and R. Peck. "Soil mechanics in engineering practice," New York: Wiley, 1967.

[26] I. Daubechies, "Ten Lectures on Wavelets." Society for Industrial and Applied Mathematics, 1992.

[27] Ensign-Bickford Aerospace and Defense. TiNi™ SCSMA Components. https://www.ebad.com/tini-scsma-components/ (visited in July 30th, 2020)

[28] sci-kit learn. https://scikit-learn.org/ (visited in July 26th, 2020)